Universität Stuttgart

Auslandsorientierter Studiengang
Wasserwirtschaft
Master of Science Program
Water Resources Engineering and
Management - WAREM

Independent Study:

Design Parameter Optimization of a Textile Turbine - Hydraulic Experiments

submitted by :

Jeffrey A. Tuhtan

Final Draft Submitted on : **May 2nd, 2007**

Supervisors : **Priv. Doz. Dr.-Ing. Walter Marx**
Dr.-Ing. Sven Hartmann

Institut für Wasserbau
Lehrstuhl für Wasserbau und Wasserwirtschaft
Prof. Dr.-Ing. Silke Wieprecht
Pfaffenwaldring 61,
D-70550 Stuttgart

INDEPENDENT STUDY FOR JEFFREY TUHTAN

"Design Parameter Optimization of a Textile Turbine – Hydraulic Experiments"

A need for inexpensive small-scale power production exists in developed nations due to the high energy production costs for large centralized plants and in developing nations where electricity may not at all be available. Wind, Solar, and Hydropower sources can aid in providing a continuous, decentralized, and ecologically-sound source of energy. The textile turbine is a new type of hydropower device which may aid in future power production.

This Independent Study provides further study of the textile turbine through hydraulic experimentation. It was carried out in furtherance of the work done by Hüseyin Eraydin in his March 2006 Master's Thesis; "Investigation on a New Type of Turbine." The primary goal of this work was to determine the optimal geometric configuration of the textile bags through laboratory experimentation.

First, a new experimental apparatus for measuring the drag force was created. Velocity profiles were then taken in the test flume for varying depth and discharge. Total drag force was then measured for stationary bags a wide variety of textile bag shapes and positions. The results indicated that multiple rectangular textile bags of the same dimensions positioned with edge-to-edge horizontal offset should provide the highest drag force. This was observed to occur almost irregardless of the longitudinal spacing. Experiments also indicated that the textile turbine gained a substantial amount of its energy from turbulent exchange. For this reason, the textile turbine's total efficiency should be evaluated using a coefficient of performance. It is also recommended that further work be carried out with the bags in motion to assess a possible reduction in system performance.

ACKNOWLEDGEMENTS

Although this report is called an Independent Study, I could not have done it on my own. Many are to be thanked, and above all others I wish to thank Priv. Doz. Dr.-Ing. Walter Marx and Dr.-Ing. Sven Hartmann for their guidance and incredible patience throughout the Independent Study.

The IWS Werkstatt Staff helped especially in constructing the experimental “Ami-Schlitten” which made my job so much easier. Thank you all.

My co-author and friend, Antonio Arenas who sometimes corrected and sometimes justified the often-occurring odd result also deserves a hearty thank-you.

And to the German Taxpayer, who foots the bill for my IPSWaT Scholarship. I am thankful for every cent I receive. And for every 27 cents I am thankful for every beer, which is surely the *only thing* Germans do better than science.

Jeffrey A. Tuhtan

May 2nd, 2007

Stuttgart, Germany

TABLE OF CONTENTS

CHAPTER 1

PREVIOUS WORK AND OPERATING PRINCIPLES

The textile turbine is the invention of Mr. Erich Kumpf from Eku Entwicklungen, GmbH. In terms of the operational theory, the fundamental groundwork has already been done. Reference will often be given to Hüseyin Eraydin's March 2006 Master's Thesis titled; "*Investigation on a New Type of Turbine*". It was in this thesis that the first theoretical work was done in assessing the textile turbine as a feasible future energy source.

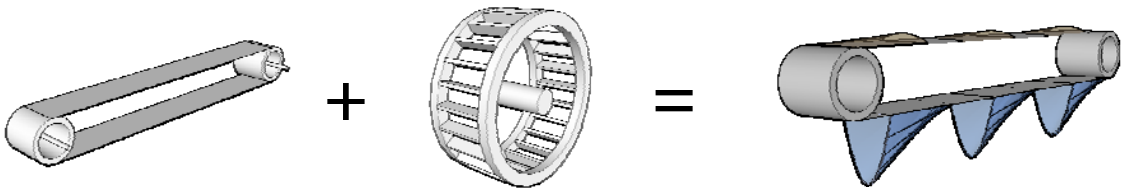

Figure 1.1: *The textile turbine can be imagined as a hybrid of two existing devices: the conveyor belt and the waterwheel.*

The main purpose of this work is to carry on where Eraydin's left off: to further investigate through hydraulic experimentation textile turbine optimization. Although there is difficulty in that it is the first turbine of its kind, concepts of previously-developed hydro machinery such as the water wheel have been exhaustively studied. This aided in providing a basis for predicting what should be expected in the operation and performance results of the experiment. Eraydin's previous work, specifically on the operational principles aided in providing at least a quantitative assessment of expected system performance. Following is a synopsis of the objectives, the basic operational principles of the textile turbine, a brief summary of Eraydin's Thesis, and comments thereto.

1.1 OBJECTIVES

The purpose of the experimental portion of the Study was to determine through laboratory-scale hydraulic analysis the behaviour of the textile bags under a variety of flow conditions. To do this, experiments were focused on the effects of bag geometry and positioning on generating the maximum drag force.

1.1.1 Tasks:

1) **Create a test apparatus for the flume which can be adapted for further experiments.**

2) **Reproduce the initial physical laboratory tests as completed by Hüseyin Eraydin using the new apparatus and compare the results.**

3) **Test various geometries and positions of the textile bags to assess their potential effect on power generation.**

4) **Provide suggestions for the optimization and operation of a textile turbine based on the results of the laboratory testing.**

1.2 OPERATING PRINCIPLES

The textile turbine can be thought of as the superposition of two existing concepts: the water wheel plus the conveyor belt. Interesting is that the marriage of a pre-medieval technology (waterwheel) to that of the Industrial Revolution (conveyor belt) results in a modern power source. Physically, the water wheel works because the energy of the moving fluid propels the blades of the wheel, centred about a fixed axis. As the wheels move about the axis it turns the axel. It is through the turning axel that gears, couplings, shafts, and pistons may be energized into motion. And it is from some novel arrangement of these objects that we can do work. Man has put into use at least four commonly-found variations of such water wheel devices. Figure 1.2 illustrates and briefly describes the working principles and maximum theoretical efficiency (η) of each case.

Essential for all of these water wheels is the fundamental concept of water's energy and how it is transferred into useful electrical energy. In this paper, water's usable energy is described in a way only an engineer could appreciate it, in terms of "head". The two most common approaches in generating electricity from hydropower and the four types of water wheels are discussed in this section.

1.2.1 Head

Head is the energy of the fluid, described in units of length. For a fluid such as water which for many practical applications has a close to constant density, an engineer can often measure the head directly. Units of length are a simple and common sense way of measuring things, even for energy. Taking a closer look at Equation 1.1 (the Bernoulli Equation), it can be seen that the total head, H [m] is made up of three constituent parts [8]: velocity head $v^2/2g$, pressure head p/γ, and elevation head z. The conversion of energy from one point in a system to another additionally includes heat, chemical reactions, system work, and anything additional the First Law of Thermodynamics will allow. These processes are lumped into the head loss term, h_l. The energy conversion in the system evolves from location 1 to a downstream location 2, where losses occur in the transition.

$$H=\frac{p_1}{\gamma}+\frac{v_1^{\,2}}{2g}+z_1=\frac{p_2}{\gamma}+\frac{v_2^{\,2}}{2g}+z_2+h_{l_{1\text{-}2}} \qquad \textbf{\textit{1.1}}$$

Where:

H is the hydraulic head (m)

p is pressure (N/m^2)

v is flow velocity (m/s)

g is the acceleration due to gravity assumed to be 9.81 (m/s^2)

z is the geodetic height above a reference datum (m)

h_l is the head loss due to friction (m)

γ is the weight density of water (N/m^3)

The production of energy using water involves two principle techniques to transfer the total head into mechanical energy in the wheel:

1) The **'big head – little flow'** scenario where the piezometric head is raised significantly at a location via a dam or weir structure. High head scenarios are also commonly found in mountainous terrain by connecting a high-altitude water source via a pipeline to a lower altitude power plant. Heads as high as 300m are often achieved using dams, and as high as 1869m with high-altitude sources [3]. It should be noted that these approaches result in high pressure systems, and often use Pelton or Turgo turbines to generate electricity. Such turbines operate through the relationship between impulse and momentum. Water from a jet under high pressure is squirted through a control nozzle onto the turbine runner blades [13]. The impulse of the water jet onto the runner is transformed to momentum of the rotating turbine, which can then be used to generate electricity.

2) The **'little head – big flow'** technique is for low-head, high-flowrate cases. This occurs most often in run-of-river schemes where a river provides a high flowrate and a large geodetic or pressure head is not available. Kaplan or Francis turbines are more commonly found in hydropower plants of this type. The general idea here is to use the large quantity of water and it's velocity head plus a little pressure head from a weir structure/barrage to generate electricity. The textile turbine fits more into this category, as it uses the velocity head of the river in order to keep the turbine bags moving.

a) η=60% ***b) η=60%*** ***c) η=71%*** ***d) η= 30%***

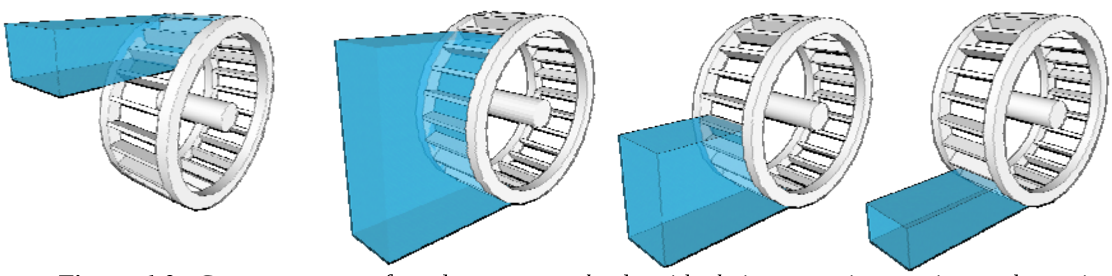

Figure 1.2: *Common types of modern water wheels with their respective maximum theoretical efficiencies* (η). ***a)Overshot b)Staudruckmaschine c)Middleshot d)Undershot***

1.2.2 Existing Types of Water Wheels

Now that two main concepts behind generating power with water have been explained, a closer look at the waterwheel variants is to be made. Figure 1.2 shows the four most commonly applied water wheels with their maximum theoretical efficiencies. Below a brief description of each type is given:

Overshot Wheel

The overshot wheel is driven by the weight of water falling on the runner blades from above. The blades are closed on the sides, making them buckets. Although overshot wheels do not suffer from the backwater problem (see the Undershot Wheel), they do have the often severe limitation that the maximum head between the inflow and outflow must be as least as large as the wheel diameter itself. This makes them unsuitable for streams and rivers with low slopes. They also tend to require more massive construction since they must withstand the weight of water falling on them. Their maximum theoretical efficiency is 60%.

Staudruckmaschine

The Staudruckmaschine works principally through use of the water's hydrostatic pressure. Although hailed as a "new" type of water wheel achieving efficiencies of up to 90%, it is nothing more than the increase of the water depth for the middleshot wheel's case. It has recently been shown [9] that it has a maximum theoretical efficiency of 60%, making it as efficient as the overshot wheel.

Middleshot Wheel

The middleshot (also called the breastshot) wheel, came as a later development than the over and undershot wheels. It was designed as a compromise between them. Water is channelled between parallel walls and strikes the runner blades ideally at the height of the wheel axle. It has the distinct advantage of overcoming the backwater problem without requiring the high head and massive construction of the overshot wheel. When it comes to efficiency the compromise pays off, providing the best maximum theoretical efficiency of the four, at 71%.

Undershot Wheel

The undershot wheel is driven by the hydrostatic pressure against the lower runner blades which dip into the downstream channel. This has the advantage that it can be used in almost any stream or channel, but has the big disadvantage that the efficiency is severely reduced in backwater conditions. Of all the water wheels, it has the greatest practical application but provides the lowest maximum theoretical efficiency, only 30%.

1.2.3 Work, Power, and Efficiency

In order to understand how we may make use of moving or standing water's energy via a big rotating wheel, a first look at the fundamental physics involved in work and power is taken. Work is the product of a force and the distance travelled by a body:

$$\text{Work}=W_{1\text{-}2}=\int_1^2 \vec{F}ds \qquad \textbf{\textit{1.2}}$$

Imagine pushing a coffee cup across a table: your hand provides the force, the cup the body, and the force of your hand times the distance the cup has travelled is the work done. In terms of a water wheel, work is performed when wheel is spinning, sent into motion. The wheel's work is used to turn the shaft about its axis; the shaft work is used to spin a magnet, surrounded by coils, generating electricity. The work done over time is defined as the power. In the coffee cup example, it is what happens if you kept on pushing the cup around instead of getting back to work. See, so you do have power at the office!

Efficiency is the ratio of how much usable power can be obtained from the total amount of available power. This Study dealt exclusively with flowing free-surface water, and the total amount of theoretically available power is calculated as the product of the pressure, flow, and efficiency. What is perhaps most interesting about the textile turbine in comparison to more conventional hydro machinery is that it also has the potential to take energy from turbulence. This means that the theoretical efficiency may calculate out at well over 100%, since the turbulent energy transfer from outside to inside the system is not included in the power calculation. It is for this reason that the coefficient of performance (COP) is used to establish the useful power output for the textile bag experiments. More details on the COP can be found in Eraydin's Thesis, and in thermodynamics textbooks.

$$\text{Power} = \text{Pressure}\times\text{Flow}\times\text{Efficiency}=\text{p}\times\text{Q}\times\eta_{\text{total}} \qquad \textbf{1.3}$$

$$\text{Power} = H_{gross}\times\rho_{water}\times\text{g}\times\text{Q}\times\eta_{\text{total}} \qquad \textbf{1.4}$$

$$\text{Efficiency} = \eta = \frac{P_{output,usable}}{P_{input}} \qquad \textbf{1.5}$$

Where:

P is power (W)

p is pressure (N/m^2)

Q is flow (m^3/s)

η_{total} is the total efficiency of the system, electrical & mechanical (unitless)

H_{gross} is the gross hydraulic head (m)

ρ_{water} is the density of water (kg/m^3)

1.3 ERAYDIN'S PREVIOUS WORK

In his March 2006 Master's Thesis, Eraydin [4] described two theoretical cases for determining the efficiency of the textile turbine:

Case 1: Using Newton's Second Law

- *Applying the principle approach of an undershot wheel with tangential wheel velocity, u, free stream velocity, v, volumetric flow rate, Q, density of water, ρ and force, F:*

$$\text{F}=\rho\text{Q}(\text{v-u}) \qquad \textbf{1.6}$$

- *Taking the derivative of Equation 1.6, setting it equal to zero and solving for the velocity which gives the theoretical maximum power: u=v/2.*

- *Using u=v/2, the density of water, and the area perpendicular to flow A⊥, now gives us the maximum power without taking efficiency into account:*

$$\text{P}_{\text{har,max}}=\rho\text{A}_{\perp}\frac{\text{v}^3}{4} \qquad \textbf{1.7}$$

- *To determine the maximum theoretical efficiency of the textile turbine, we need to also determine the total power capacity of the water in the flume:*

$$\text{P}_{\text{kin,flow}}=\rho\text{A}_{\perp}\frac{\text{v}^3}{2} \qquad \textbf{1.8}$$

- *This results in an* ***upper limit of theoretical efficiency as being 50%*** *based on calculations used in determining the Undershot Water Wheel's efficiency.*

Case 2: Application of a Resistance Formula

- *Assume a force due to pressure drag acting on the textile bag, similar to that of the undershot wheel. C_d is the experimentally-obtained drag coefficient, ρ is the density of water, $A_\perp$ is the area perpendicular to the flow direction, v is the free stream velocity of the water, and u is the velocity of the submerged object. For both Eraydin's and our work, u=0 for all experiments since the apparatus was kept stationary in the flume :*

$$F_d = \frac{1}{2} C_d \rho A_\perp (v-u)^2 \qquad \textbf{1.9}$$

- *Once again, take the derivative of Equation 1.6, using F_d=F to obtain the velocity which gives the theoretical maximum power: u=v/3.*

- *This results in a new performance ratio which is convenient to use, since we can write everything simply in terms of our experimentally-obtained C_d (for the complete derivation of Equation 1.10, see Eraydin's Thesis):*

$$COP = \frac{P_{har,max}}{P_{kin,flow}} = 0.148 C_d \qquad \textbf{1.10}$$

In the end, a set of single and dual bag experiments were run to determine the force generated by the textile bags. A prototype of 11m long and 80cm wide was used in river experiments, but a smaller scaled-down model was used in the IWS flume. To remain as consistent as possible with the previous work, experiments were run with the same flume and similar conditions to Eraydin's.

1.3.1 Single Textile Bag Results

Experimentation was conducted using a 40cm wide parabolic bag set. Mean flow velocities in the flume ranged from 30-60cm/s. Depth-varying velocity profiles were not obtained, most likely since the apparatus was made such that the best bag position would be close to or at the surface. Drag coefficients for a single bag remained close to constant through a range of Re at C_d=3.2, indicating complete boundary layer separation, and justification of using the Euler Model Law. The amount of force obtained from the single textile bag setup ranged from 4.09-22.38 N with varying discharges of 40-160 l/s, respectively.

1.3.2 Single Metal Bag Results

A stiff metal triangular bag was also used. C_d was raised for the same flow conditions and obtained an average value of 4.2. Forces generated ranged from 7.83-37.22 N with varying flow rates of 70-160 l/s, respectively.

1.3.3 Dual Textile Bags

Experimentation with two textile bags of the same dimensions as that of the first showed that when the bags are moved further apart, there is a general trend which shows an increasing total drag. The range C_d for the two textile bags was 3.46-5.87 for length to bag height ratios of 0-11, respectively. Forces generated ranged from 19.83-29.81N with a constant flow rate of 90 l/s.

1.3.4 Performance Results

Power ranging from 242 to 520 W was obtained from the prototype. A reduction factor for the whole system drag performance was also introduced. Since it was found that energy from outside the control volume enters the system via turbulent exchange, the COP was recommended to indicate system performance. COPs of up to 170% were observed for the experiments, and the maximum power production was found to occur at x/h of 2, with a production of 626 W. This occurred with two textile bags spaced on centre one meter apart and with a corresponding C_d of 11.7.

1.4 COMMENTS

Although Eraydin's Thesis provided a sound technical background for future work, it left many questions unanswered. We now know that the equations used to calculate water-wheel efficiencies will not lead to satisfactory results when applied to the textile turbine due to the turbulent exchange. Additionally, the previous experiments carried out did not try to first optimize the shape of the bag, it was assumed that a parabolic shape would be the best. This may or may not be the case, and should be looked into. A key assumption made was that the drag force is primarily dependent on increasing distance between the bags. Offsetting the bags horizontally from one another may also be another option. Lastly, there was no attempt to utilize that part of the vertical velocity profile which has the highest value. Our work intends to find the "sweet spot" of the flume and use this, as the differences in the velocity profile can greatly help in increasing the overall efficiency of the textile turbine.

CHAPTER 2

GEOMETRIC CONSIDERATIONS

The purpose of this section is to provide a brief discussion of the important dimensions and geometric limitations of the experimental setup. This is the first step in understanding the project parameters. Engineers can often simplify problems to the one-dimensional case, while nature assuredly acts in all three. A Cartesian coordinate system following the convention shown in Figure 2.1 was chosen to make the experimental setup as easy as possible to follow. Note that the axes are color-coordinated. Blue (x) is used for the dominant flow direction, red (y) is along the direction of the characteristic length of the bag, and green (z) represents the depth in the flume.

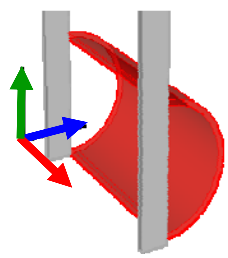

Figure 2.1: *Experimental coordinate convention. The red area represents a parabolic textile bag placed normal to the flow direction.*

2.1 CHALLENGES FACED BY DIMENSIONS AND BOUNDARIES

In this section, important dimensions and boundaries are discussed. For the hydraulic model used in the IWS flume the most important experimental data can be found in Table 2.1. The most important set of dimensions are those of the flume and those of the prototype. The dimensions of the flume used in the IWS research facility represent the physical limits of the experiment, and those of the textile bag represent a scaled-down version of the full-sized prototype. This gave the geometric boundary conditions for the numerical model, and imposed limits on the sizing of the experimental apparatus. It was important to find out how large the textile bags could be made without the influence of the sidewalls affecting the experiment. This information was obtained using velocity measurements. It was also crucial to obtain an idea of what shapes might be the most suitable. Each shape provided its own unique set of limitations when considering it for use in the experiments. To keep the experimentation as fundamental as possible, only the most geometrically simple shapes were used. Choosing an appropriate length factor L_r, the ratio of the prototype characteristic length to that of the model, was also a difficult task. It was assumed that the experimental apparatus should allow textile bags of the same dimensions as those used by Eraydin [4]. Further discussion on this can be found in Chapter 3. Figure 2.2 depicts flume dimensions and textile bag positioning during experimentation.

Table 2.1: *Important Geometric Properties of the Experiment. *In both cases, a wide variety of sizes were tried in order to find the maximum drag at different depths in the flume.*

Property	Length (x) [m]	Width (y) [m]	Height (z) [m]
Flume	>10m	1	0.54
Textile Bag, L_r 5	0-0.155*	0.4	0.02-0.268*
Textile Bag, L_r 10	0.034-0.125*	0.2	0.087-0.155*
Wagon	1.95	1	0.2
Max. Flow Depth	-	-	0.48
Min. Flow Depth	-	-	0.28
Min. Measuring Dist. ADV	0.1	0.1	0.1

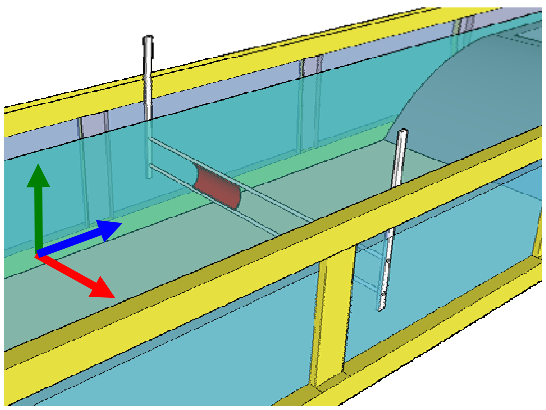

Figure 2.2: *Positioning of the textile bag experiment in the IWS flume. The positioning rods allowed two degrees of freedom: the bags can be moved either horizontally or vertically within the flume.*

2.2 USING GEOMETRY TO MAXIMIZE THE DRAG FORCE

The height and width were the two most important bag dimensions in that they define the planar surface perpendicular to the flow direction. To optimize the textile turbine, the maximum drag force was sought out for fixed flow conditions, bag dimensions, and bag flume position. Consideration was given especially to shapes which can be easily implemented on the experimental apparatus, and for which known experimental data exists. Hydromechanics theory provides that maximizing the area perpendicular to flow will help to do just that. An especially important geometric property is that the textile bag has a generally *simple shape*. This is not a design for a space shuttle or F-1 race car, after all. It should be cheap to produce from an environmentally-friendly textile material and easy to replace and repair when damaged or destroyed. Shapes investigated in this section had either rectangular or circular areas perpendicular to the flow direction. The best shape should be relatively simple to construct and provide the largest amount of cross-sectional area for a given perimeter. Three choices of rectangles were used, (Figure 2.3) where rotation about the y axis 90° would be fully vertical. The results are shown in Figure 2.4, which depicts total perimeter length vs. the ratio of area to perimeter.

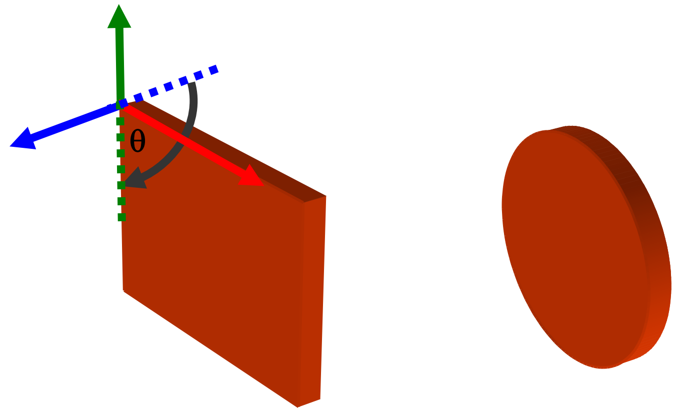

Figure 2.3: *Simple shapes used to compare possible bag designs depending on their area to perimeter ratio. Rectangular shapes were rotated about the red (y) axis.*

It should be noted that these basic shapes were chosen because of their geometric simplicity, and their ease of construction. The relation of area to perimeter is important in that it gives a qualitative relation of which of the drag force components will be most active. Drag due to pressure is dependent on the surface area, whereas viscous drag is a more likely a product of a body's perimeter. Literature [16] indicates that for the shapes investigated, the highest drag coefficients occurred at high Reynold's Numbers, where boundary layer separation occurs, and the total drag is mainly due to pressure. From literature, it was found that the best performing drag coefficient of 2.9 is obtained from a rectangle with a w/h ratio of 0.65. A semicircular shell performs close, with a drag coefficient of 2.3. To give a practical idea of the drag coefficient in practice, a comparison can be made to the Honda Insight Hybrid's C_d of 5.10 to that of the Hummer H2's C_d of 26.3 [15]. Aesthetics aside, the geometry clearly plays an important role.

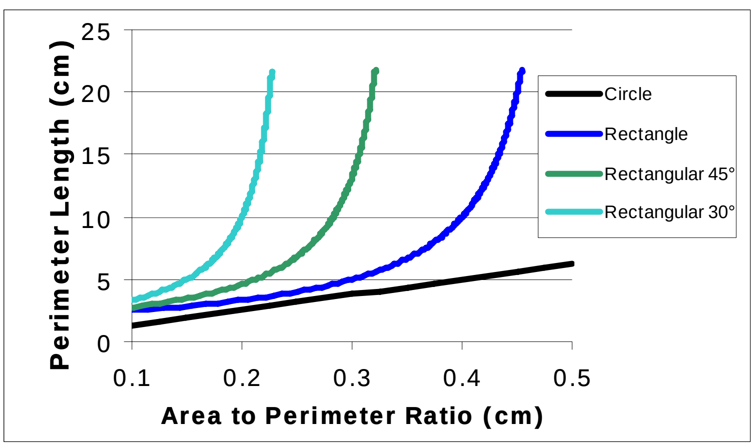

Figure 2.4: *Perimeter Length versus the A/P ratio. The circle is the most 'efficient' shape, and a decreasing angle from the vertical greatly reduces the increase of a rectangle's A/P.*

2.3 CHOSEN BAG SHAPE FOR EXPERIMENTATION

From the results of the simple exercise in geometry, it was determined that the optimum bag shape should not have a circular or parabolic perpendicular area, but rather rectangular. Additionally, rotating the bag about the y-axis would not seem to yield better surface area to perimeter ratios. For these reasons, it was decided to focus the experimental investigations on textile bags having rectangular areas perpendicular to the flow. The experimental apparatus allows that the rectangle be projected into the flow direction for a wide variety of parabolic shapes. The experimental investigations were therefore carried out on flat rectangular and parabolic textile bags. In the next chapter, further theoretical investigation of these shapes is made, and bag sizing is chosen. Additionally, a look into the theory behind the bluff body drag is made to see how the chosen geometry might affect flow around the textile bag. Going back to the basics of hydromechanics was important to find out what could be expected, but wasn't necessarily what was found.

Figure 2.5: *Which would you drive? Honda's Insight Gas-Electric Hybrid with C_d=5.10 or General Motor's Hummer H2 with C_d=26.3?*

CHAPTER 3

HYDRAULIC THEORY

Reviewing the subject of flow around bluff bodies was essential to obtain an idea of what shapes and under what conditions the highest drag forces could be obtained. First, the drag force on bluff bodies and the contributing factors which are particularly relevant to the Independent Study model are examined. Next, boundary layer theory, its principle equations and relevance to the flow regime around the textile bags is outlined. Important to the discussion is determining the range of Reynolds Numbers which are both reproducible on the laboratory scale and which are found in nature. A brief examination of two-dimensional potential flow around bluff bodies is then given. Following is the application of a numerical model of potential flow to visualize the pressure distribution around the textile bags. Finally, fixed bag shapes and dimensions for the experiments are chosen based on the findings of this and of the previous chapter.

3.1 DRAG FORCE DUE TO FLOW AROUND A SOLID BODY

3.1.1 Incompressible Flow Assumption

The drag force due to flow around an object depends on the body's geometric properties, the flow field direction, and the Mach number for compressible flow, Bohl [2]. In overpressure zones with compressible flow, flow lines are forced closer to one another due to the physical compression of the fluid, and for under-pressure zones, due to expansion of the fluid, the flow lines move a little further apart from one another. Shockwaves due to purely under-pressure flow do not occur. Since the flume water surface in the Independent Study is exposed only to atmospheric pressure, and the water remains at a relatively constant temperature of 17°C, the effects of compressibility on the flow around the textile bags are neglected.

3.1.2 Total Drag Force

The drag force imparted on a stationary body, $\mathbf{F_d}$ within a flowing fluid can be formally described as the sum of two components; the body force $\mathbf{F_b}$ and the surface force $\mathbf{F_s}$.

$$\underline{F_d} = \underline{F_b} + \underline{F_s} \qquad \textbf{3.1}$$

In this Independent Study, the only body force considered was the force due to gravity; the Coriolis force, and centrifugal forces are neglected. Since the body force acts only in the negative z-direction, it plays no role in the determination of the drag force in which we are interested, $\mathbf{F_{dx}}$. This is the case since the size of the textile bags used during experimentation were mostly vertical and could hold very little water (<<1 liter). It is worth mentioning that for a full-scale prototype, the weight of the filled textile bags will be important in the design and operational of the textile turbine, since the stability of the platform will depend on the weight and positioning of the bags.

The remaining force components of the surface force can be described in integral form as the total stress acting on the surface, σ integrated over the surface *dA*:

$$\underline{F_d} = \oint \underline{\sigma} dA \qquad \textbf{3.2}$$

To put this integral form into practical use, the stress vector is split into two principle components, one tangential to the body surface, σ_t and one normal, σ_n.

$$\underline{\sigma} = \underline{\sigma_n} + \underline{\sigma_t} \qquad 3.3$$

For an incompressible, Newtonian fluid the normal stress component can be expressed as the sum of the pressure at the surface, p and the force due to viscous shear:

$$\sigma_n = \left| -p + 2\eta \frac{\partial v_n}{dn} \right| \qquad 3.4$$

Where pressure is always taken normal to the body surface and n is the normal coordinate to the body surface with v_n as the velocity component in this direction. In the case of a parallel flow field around a submerged body with its top edge at the surface, and having a small vertical velocity component, the second part of the equation can be neglected. In the Independent Study, the assumption was made that the pressure is the only normal force component on the textile bag's surface. Thus a stationary vertical bag acts as a flat plate, and the resulting viscous shear force acting normal to the surface is assumed to be zero. Geometries which extend in the x-direction will incur higher viscous shear forces, but the magnitude is assumed to be small and is neglected.

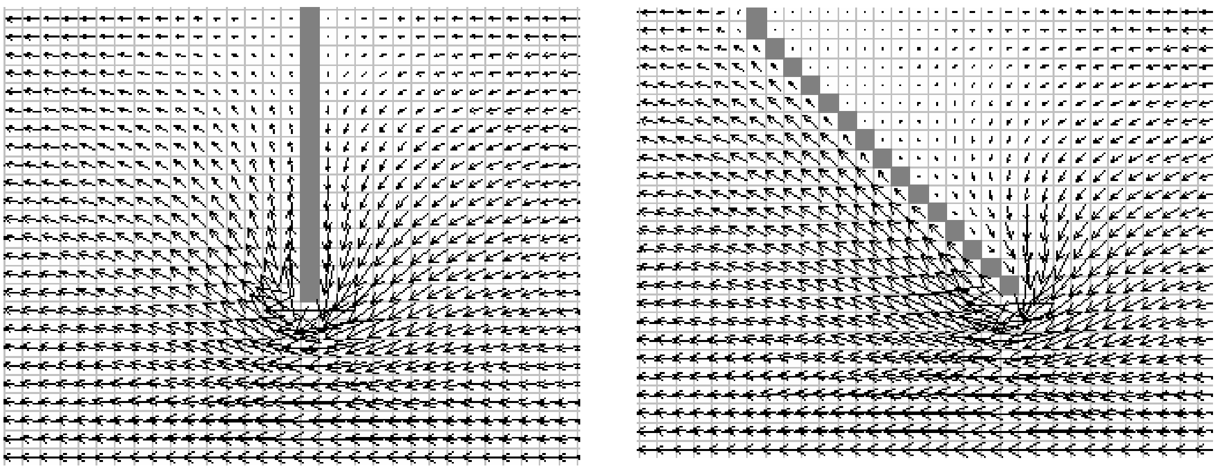

Figure 3.1: *Velocity profiles for:* ***Left****, for a flat vertical plate.* ***Right****, for a slanted plate. Both examples included identical boundary and initial conditions. Note that the slanted plate design results in a significantly higher "dead water" region. This is expected to result in less turbulent exchange, and thus was determined to not be a suitable design candidate.*

The tangential component as the viscous shear can be written as:

$$\sigma_t = \tau_w \qquad 3.5$$

From the previous assumptions, the *normal component* is now referred to as only the **pressure force**, and the *tangential component* as the **friction force**:

$$\underline{F_d} = \oint \underline{\sigma_n} dA + \oint \underline{\sigma_t} dA \qquad 3.6$$

3.1.3 Pressure Force

$$dF_{wp} = p_l dA \qquad 3.7$$

The component of the force in the flow direction where α is the deflection angle of the submerged bluff body measured from the horizontal is then:

$$dF_{wp,x} = p_l \cdot dA \cdot \sin\alpha \qquad \textbf{3.8}$$

Integration of this equation over the surface of the body is possible using the velocity field calculated via the energy equation or by using numerical methods. This equation can be applied when the upstream distribution of external pressure and velocity is known. A hydrostatic pressure distribution was assumed, and velocity field measurements were obtained experimentally.

3.2 BOUNDARY LAYER THEORY

At the front of the body near to the point of stagnation a thin, slowly flowing boundary layer in which laminar flow is present. Along the body, the boundary layer increases in thickness, and a transition from laminar to turbulent flow occurs. For a long, thin body oriented parallel to the principal flow direction the boundary layer covers the entire surface.

This Study focused on the potential effects of boundary layer development on flow around a body such as a flat plate whose area is facing perpendicular to flow. For such cases, the laminar boundary layer occurs in the vicinity of the stagnation point. Turbulent boundary layer development depends on the flow characteristics, (Re). Close to the body itself the flow is accelerated, causing the streamlines to converge. The boundary layer lies inside the positive pressure gradient zone around the body. Since the bag has a parabolic shape when filled with water, changes of the boundary layer separation point will occur depending on the parabolic shape and the flow regime. This in turn will result in a change of the flow characteristics around the body itself. As the change occurs, streamlines diverge and the pressure in the immediately surrounding flow field and in the boundary layer will drop. Should a bend or angle be abrupt, the boundary layer will separate from the body at that point. At the separation point the velocity gradient at the surface is equal to zero. Boundary layer separation causes an eddy-filled dead water zone in which backflow takes place.

3.2.1 The role of boundary layer separation on the textile turbine

Prandtl [16] has provided an interesting experiment which gave a clue about how to optimize the shape of the textile bags: for flow around a sphere, Prandtl artificially increased turbulence on a sphere via a metal ring placed slightly in front of the region of lowest pressure on the sphere. The resulting turbulent boundary layer increased in velocity through transverse exchange with the surrounding flowing fluid and could therefore withstand a larger pressure increase before boundary layer separation was created. In this case the viscous drag increased for two reasons: the wall shear stress in the turbulent boundary layer was now greater, and the distance along the body before separation was also increased. Surprisingly, *even with a larger contribution of the viscous drag, the total drag force on the body was decreased!* This indicated that the pressure drag decreased at a higher rate then that at which the viscous drag was increasing. The reasoning behind this phenomenon is that the pressure in the dead water area remained close to constant and therefore approximately the same as the pressure at the point of separation. This means that for turbulent boundary layers, displacing the point of separation to a location after the maximum cross-sectional area can increase the pressure in the dead water zone, thus reducing overall pressure drag on the body. In Figure 3.2 the separation of the boundary layer from a circular smooth bluff body and for a pitted golf ball is shown. For the smooth ball, the pressure drag is highest since the boundary layer separates at the point of maximum width. This results in the streamlines downstream of the separation point having the widest spread in the wake region, and thus the lowest pressure. The pitted ball however forces the turbulent boundary layer to separate past the point of maximum width, reducing the pressure drag. This effect can be seen in Figure 3.2. In the Independent Study, the maximum pressure drag is desired, and so the boundary layer separation should occur at the point of maximum width.

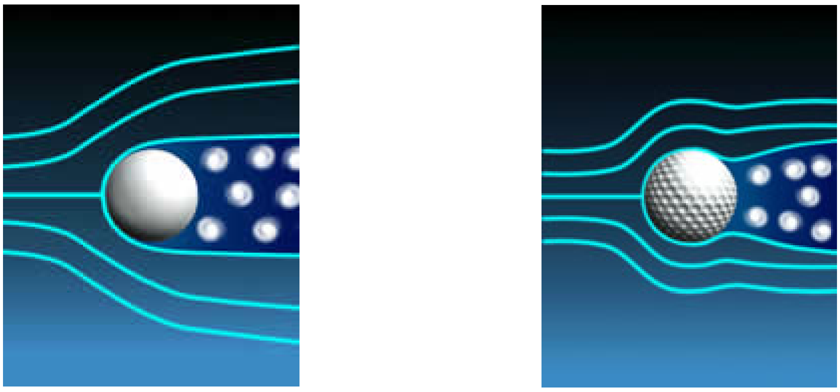

Figure 3.2: *Streamlines, boundary layer separation, and turbulent wake for a circular shape. Notice the difference in location for the point of separation. Picture from the University of Southampton* [14].

To assess the exact effects on the textile bags of a parabolic shape operating under transitional Re was not possible for this Study. This is because determining the exact location of boundary layer separation even for the steady-state case experimentally was simply too difficult. It is for this reason that future designs should include a "turbulent edge" on the top and bottom of the textile bag design to ensure boundary layer separation at a specific location. The assumption is that defined boundary layer separation at the location of the maximum cross sectional perpendicular to flow will then maximize the contribution of the pressure drag.

According to Prandtl and Blasius [16], it is possible to experimentally determine the energy loss due to the formation of a turbulent boundary layer on the textile bags. For this Study it was assumed that the amount of energy converted due to skin friction drag is very small and was neglected; only the pressure drag was used.

3.3 TWO-DIMENSIONAL POTENTIAL FLOW AROUND BLUFF BODIES

The macroscopic flow field around a body is dependant mostly on the body shape itself [16]. Thin plates or streamlined bodies whose long axes are parallel to the flow direction have streamlines which may close at the end of the body. Compact and angular bodies develop an extended dead water region behind them. Before experimentation was carried out, possible bag geometries were considered based on theory, and tested for pressure drag using a simple 2D potential flow model.

3.3.1 Potential flow formulation

Bohl [2] provides a good mathematical explanation of 2D potential flow with respect to a circle. It it was good beginning point for the Independent Study: a circle is a simple and physically sensible configuration, mathematically it serves as an example for superposition, and technically it is the basis for the calculation of the flow around a submerged body.

Potential flow can be described through superposition of a parallel flow along the x-axis with a dipole and rotational flow components. The velocity field itself is then considered irrotational, and can be described as the gradient of a scalar function. This allows force fields to be derived from the potential, i.e. the pressure force can be derived by looking at the change in potential due to the widening and narrowing of streamlines surrounding a body. The potential flow function, based on superposition can be described as the additive quantity of its individual components:

$$w(z) = cz + \frac{M}{2\pi}\frac{1}{z} + \frac{-i\Gamma}{2\pi}\ln\frac{z}{R} \qquad 3.1$$

Where c, M, Γ, and R are real constants and z is the depth.

The potential flow function for a circle can be more easily used after transformation into polar coordinates:

$$W(\varphi) = \left[\left(cr + \frac{M}{2\pi r}\right)\cos\varphi\right] + i\left[\left(cr - \frac{M}{2\pi r}\right)\sin\varphi - \frac{i\Gamma}{2\pi}\ln\frac{r}{R}\right] \qquad 3.2$$

From this it can be shown that the potential function, $\Psi=0$ when $r=R$ and at the same time the dipole moment $M=2\pi R^2 c$. This means that the circle with radius R is also a potential line. The stream function $w = 0$ when $r = R$, and at the same time, the dipole moment $M = 2\pi R^2 c$. This means that a circle with radius R is now itself also a streamline. That the velocity field of the dipole moment and the potential vortex for abs(z) approaching infinity disappears, leaves at r=R only the contribution of the initial parallel flow field.

The significance of this formulation is that streamlines can then be plotted perpendicular to the equipotential lines, where the difference between streamlines gives the volumetric flowrate (for incompressible fluids). This allows for the creation of a simple flow net which can show at least qualitatively the expected behaviour of flow around a body. The main drawback to using potential flow is that not all real world flow characteristics are included. For instance, the effects of turbulence and boundary layers cannot be taken into account. In this Study, potential flow was used to aid in assessing which bag geometries in the x-z plane may be good candidates for further hydraulic experimentation.

3.3.2 ASMWIN bag shape trials

Neglecting the effects of turbulence and the viscous shear component of drag, the pressure component of the drag force can be assessed through the use of a 2D potential flow model. The idea was not to calculate directly the expected values of pressure, but to use potential flow to assess qualitatively which bag geometries might produce the best results. Of most interest was the shape of the potential pressure field directly in front of and in back of the simulated bag profile. The greater in magnitude the difference in the pressure field, the better this configuration was as a candidate for use in the experimental work.

Several bag geometries were tried out using ASMWIN, a 2D flow and transport program for groundwater. Assumptions were steady-state conditions and an incompressible Newtonian fluid. A finite difference method was used with a domain of 100 x 50 grid cells; each assigned a unit width and height. Boundary conditions were set such that the upper and lower edges of the domain were no-flow, constant head on left, and constant flow on the right. The bag opening height for all cases was set to 30 cells. Cholesky decomposition was used as the numerical solver. The computational time, being less than 10 seconds for most simulations did not play a significant role.

The model was first run without the bag's presence to ensure that the resulting flow field and pressure gradient were without numerical error. Next, various combinations of bag profiles were input, where the shape of the bags were outlined by assigned cell-by-cell no-flow boundary conditions. After each model run, the data were saved as Surfer files, and imported to view. The initial no-bag pressure gradient was then subtracted from each case to qualitatively determine a particular geometry's effect. Using Surfer, the values were then gridded onto a 100 x 50 cell colormap, to visualize the resulting pressure distributions at the same resolution as the model, and to observe possible interpolation errors and boundary condition effects.

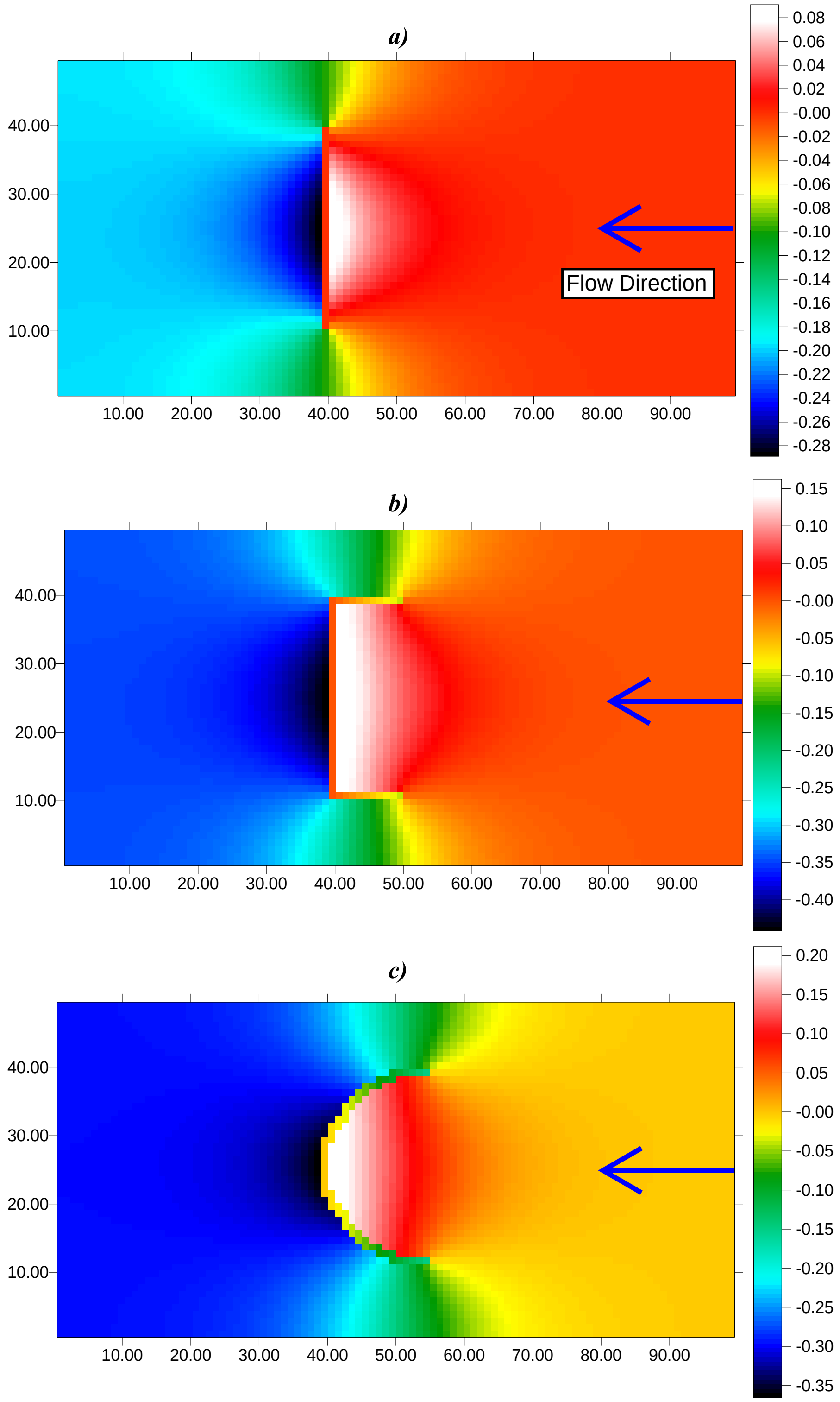

***Figure 3.3:** Pressure distribution from potential flow calculations.*
a) flat plate Δp= 0.09 b) box shape Δp=0.27 c) semi-circular curve Δp= 0.22

Several combinations of hyperbolas, rectangles, boxes, triangles, flat planes, and inclined planes were tried. In general, the best performance came from the box shape and the semi-circular curved bag shapes (see Figure 3.1).The experimental apparatus only allowed for inclined plates and curved surfaces normal to the flow direction. It was for this reason that a parabolic bag shape was chosen for the experiments.

In addition to determining the velocity as it varied with depth, we are interested in obtaining the three-dimensional velocity distribution in the flume with and without the textile bags in order to better understand the pressure distribution in front and around the side of the bags. Due to the time required to carry out the velocity field measurements, only one scale factor of $L_r = 10$ of the textile bag is used for the fully three-dimensional velocity field.

Since the positioning of the textile bags is based upon the desire to generate the largest drag force possible, we are interested in engaging our textile turbine in the region corresponding to the highest flow velocity. A preliminary study of the drag force generated by a single textile bag as discussed in Chapter 4 indicated that the most productive region in the flume is located by a submersion of the top of the textile bag of at least 5 cm. This makes sense, since we can see that there is a slight decrease in the flow velocity at the water surface caused by friction at the water-air interface. Important also was that the maximum flow velocity has a typical turbulent flow profile, where the maximum velocity is constant over a portion of the flume's depth. The range of Re we use during experimentation is for the fully-turbulent flow condition, as discussed above. It can also be assumed, (but should be verified through field measurements) that in a natural system a similar flow regime takes place.

To describe the vertical velocity profile of the flume, we compare the experimentally-obtained profiles to calculated values. We can much more efficiently model the performance our textile bags through the use of a CFD program than we can by running physical experiments. It is for this reason, that it is important to be able to derive mathematical relationships for velocity profiles used in the CFD analysis which were not measured directly.

CHAPTER 4

LABORATORY EXPERIMENTS

This section describes the procedures and results of the hydraulic experiments. First, a discussion of the flume and its velocity profiles for various conditions is discussed. Following is a section providing the drag force results for single and multiple bags. Next, the most important results are collected and analyzed for the investigated dual and triple bag configurations. Finally the relative error in these experiments is compared to that of Eraydin's.

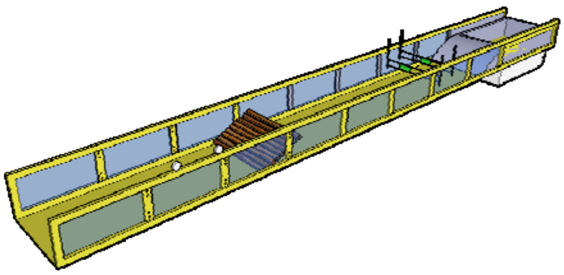

Figure 4.1: *schematic representation of the Flume, "Big Yellow". Width of 1m, max flow depth 0.5m, max flow rate 180 l/s.*

4.1 THE FLUME

Throughout the experimental process a single flume at the Institute for Hydraulic Research, University of Stuttgart was used. The flume dimensions can be found in Chapter 2. In this section velocity measurement and the resulting vertical velocity fields under a variety of operating situations are discussed. It was important to the optimization of the textile bags that the ambient conditions were well established so that they could transfer as easily as possible to the numerical model. Understanding the flow field required taking a large quantity of point velocity measurements at various spatial and temporal resolutions. This was done to find the best resolutions in terms of accuracy and precision, and to optimize the quantity of measurements needed for future studies using similar equipment. Fundamental to the experimental work was determining the vertical velocity profile as it related to the positioning of the textile bags under submerged conditions. Another important factor was the identification of any irregularities in the flume flow field.

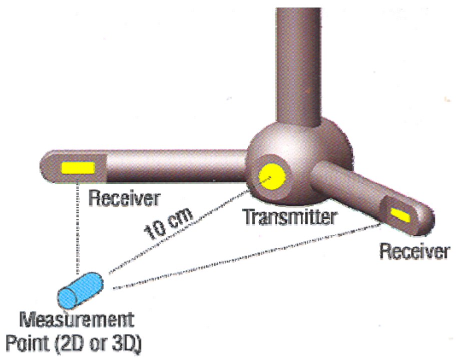

Figure 4.2: *schematic representation of the ADV. The Flow Tracker Handheld version which also measures the velocity field in the z-direction was used.*

4.1.1 The Wagon

In order to carry out the experiments as accurately an easily as possible given both the wide range of configurations and the physical restraints on using the flume itself, it was necessary to first design a simple and reusable experimental apparatus. Initially, the hope was that the wagon itself would be able to roll along top of the flume, thus the power generated by the bags in motion (but not in rotation) would be able to be directly calculated during the experiments. Unfortunately, due to horizontal bracing elements required to hold the flume together, this was not possible. Furthermore, the elements limited the total feasible length of the experimental apparatus to 1.95 meters in length.

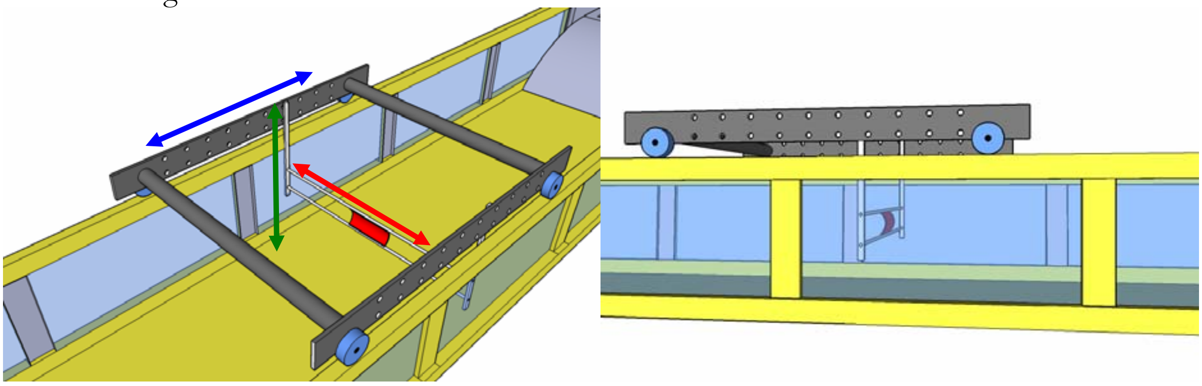

Figure 4.3: *schematic representations of the experimental apparatus. The arrows indicate the degrees of freedom for bag positioning.*

The resulting apparatus was 1.85 meters in length and consisted of a steel frame having four low-friction bearing wheels. Along each side of the frame were drilled two sets of vertical holes, spaced 10cm on center. From these holes, vertical bracing bars were mounted to hold the textile bags. The bags were then positioned on two sets of identical horizontal metal extenders having roughly the width of the flume itself. Thus the positioning of the textile bags in the flume was able to be varied in all three dimensions and at the same time allowed for a stable bag configuration throughout. Drag force measurements were also taken in the purely horizontal direction, as in the previous experimentation by Eraydin [4], the drag force was taken at an angle to the vertical, adding possible additional error.

Setup of the experimental apparatus was straightforward: First, the bags were cut and positioned on the horizontal extenders relative to the center of the flume. Next, the vertical bracing bars were positioned such that multiple bags had a fixed measured distance from one another. Finally, the bags were positioned via the extenders onto the vertical bracing bars such that the required bag depth and opening height was achieved in each case.

It is worth noting that the experimental device did provide some resistance to the drag force, and was found to be 0.15N though a series of 60 measurements. The rolling friction was calculated by applying a horizontal force on the stationary device when no flow was in the flume. At the moment in which the wagon began motion, the force was recorded.

4.1.2 Velocity Measurement

A Acoustic Doppler Velocimeter (ADV) was used for velocity calculations in the IWS flume. Operational details of the device are described in detail in Eraydin's Thesis work. Important to note about the ADV are two things: that it samples at 10 Hz, and that the samples are taken 10 cm in front of the device itself (see Figure 4.2). The first factor plays an important role in indicating the statistically relevant sample size, which then gives the experimenter an idea of how much time is required for measuring each point. Furthermore, because the device measures at a distance of 10cm, it can be used to measure close to the textile bag surface with reasonable accuracy (~1%), while at the same time not affecting the flow field around the bag.

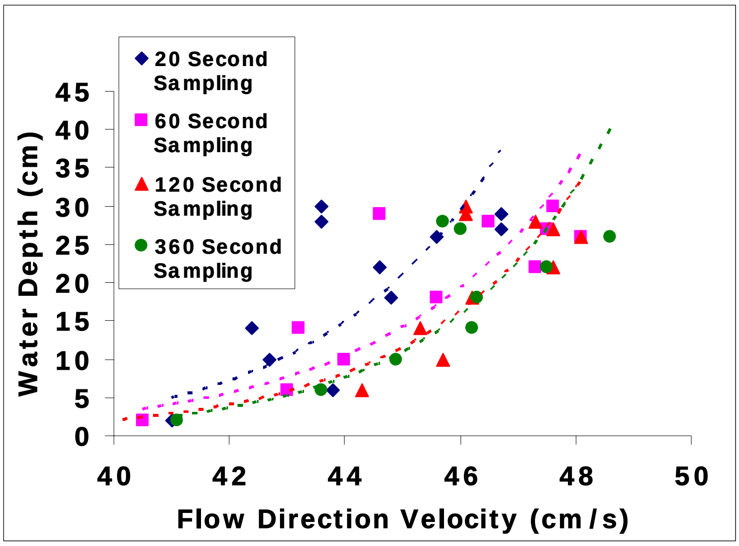

Figure 4.4: *Variation of velocity profile versus the time of point measurement. Note that 120 second and 360 second samples result in essentially the same point averaged velocity profile. This corresponds to a per point sample size of 1200 and 3600 values respectively.*

4.1.3 Vertical Velocity Profiles

Contrary to literature, the vertical velocity profiles even in a reasonably well-controlled flume were often not what were expected for a simple turbulent flow case. Most importantly, the assumption of a uniform velocity profile close to the walls (<10cm) should not be made. This restricted then the horizontal positioning of the bags, and helped reinforce the decision to use a

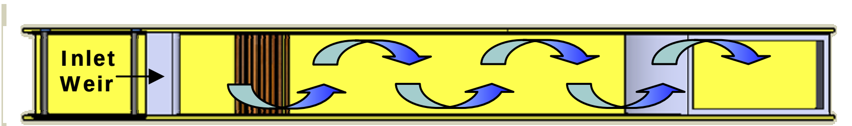

Figure 4.5: *Plan view of the flume. The Flow direction is from left to right. The curved arrows indicated the observed internal wave motion with its assumed periodic-like behavior.*

larger L_r to shrink down the dimensions so that more room to horizontally offset the bags could be made. Additionally, it should be noted that the flume in general appears to have an internal serpentine wave motion in the horizontal which causes alternately higher and lower mean flow velocities, depending on the position along its length. This was most likely caused by waveforms generated by the initial outflow over the weir structure with its corresponding hydraulic jump. It is recommended that a honeycomb flow straightener be installed near the inlet weir to remediate some of this effect.

Velocity measurements in the flume were taken for a range of flow rates and depths to determine both the available Re in the flume and to locate the optimal position for the textile bag (this was assumed to be the location with the highest flow velocity). The ADV was placed in the horizontal centre of the flume to obtain the profiles, while varying the flow rate and depth. Additionally, in order to help in the calibration and verification of the numerical model, it was important to determine the velocity profile in three dimensions. This was done for principally two reasons: The first being that the magnitude of energy imparted onto the textile bag via turbulent exchange varies with the velocity in each direction. Secondly, that when the velocities can be compared relative to one another, optimization can be more readily achieved. A last series of velocity measurements were carried out in front and in back of the textile bag to estimate the magnitude

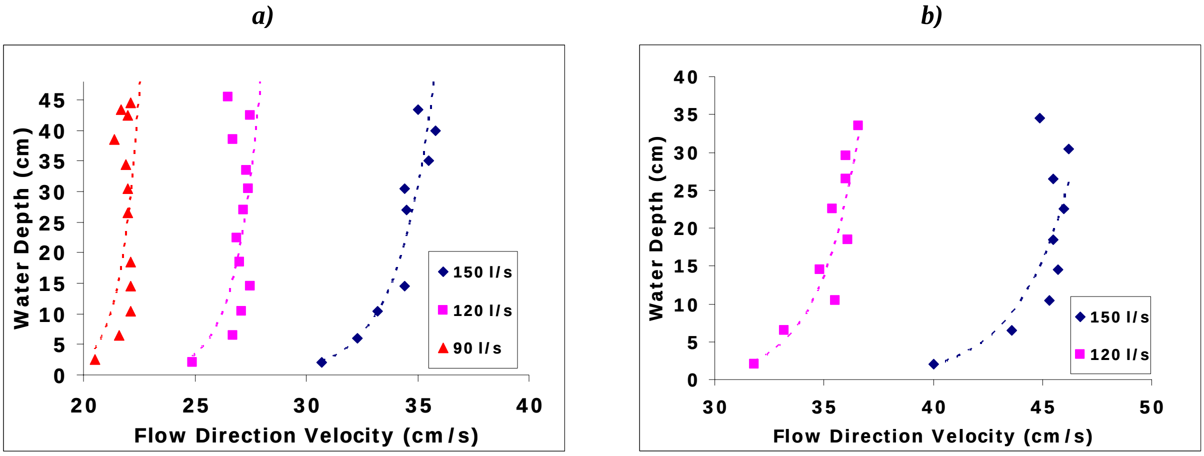

Figure 4.6: *Velocity profiles in the flume varying flow rate and depth.* ***a) depth of 48cm b) depth of 38 cm.*** *Note the relatively flat front of the flow profile due to turbulence and the reduction of the flow velocity near the water surface.*

of the velocity fluctuations in three dimensions to aid in the numerical model's k-ε parameter estimation values. The most important result of the velocity profile measurements was the result that the textile bag should be submerged into the area of highest longitudinal velocity to achieve the best expected performance. Previous prototype designs, and indeed the work of Eraydin had the bags at the water' surface, and thus were not able to extract the maximum energy. In keeping with this, experimentation was done with single bags, varying both their dimensions and their vertical position in the flume to determine which combination of variables might produce the best drag force.

4.2 TEXTILE BAG DRAG FORCE

After obtaining a wide range of velocity profile data for the flume it was determined where the most suitable horizontal and vertical positions of the textile bags should be. The next series of experiments, as mentioned in the previous sub section were carried out to calculate the drag force. In his previous work, Eraydin had chosen to use a parabolic bag shape. In this work, it was decided to use a primarily rectangular bag shape, since it provides the maximum theoretical drag coefficient for a given cross sectional area. After Parkinson and Yeung [12], it can be assumed that the maximum drag coefficient, C_d is 2.9 for a bag in which the height of the bag is 0.65 that of its width. Here it is also worth mentioning that Eraydin found values of up to 11 for his parabolic bag shape. A variety of experiments with an L_r of 5 and 10 were carried out to determine the maximum drag force due to shape, the number of bags and flow field-dependant considerations.

4.2.1 Choosing L_r

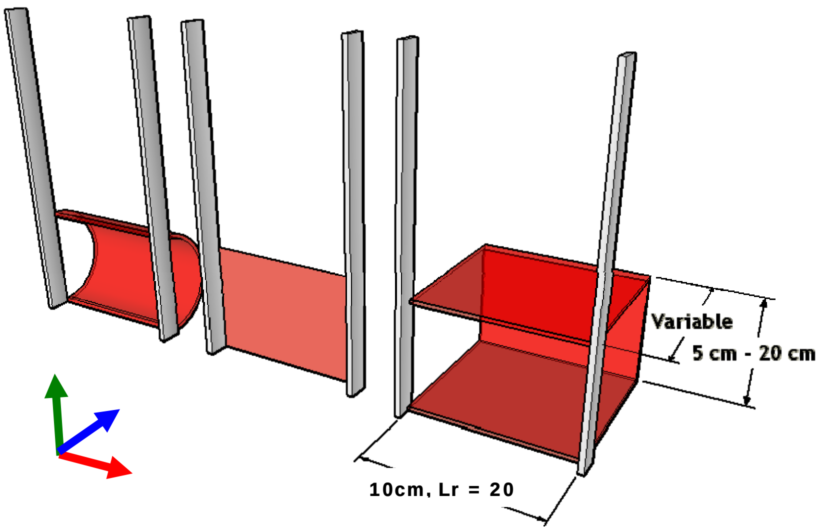

Figure 4.7: *Possible bag configurations for use in the laboratory experiments. From left to right: Parabolic, Flat Plate Rectangular, Square.*

Due to the experimental apparatus and the limitations due to the size and maximum flow rate of the flume, it was necessary to scale down the dimensions of the textile bags. At first, it was looked at using an L_r of 5, (following Eraydin) and assuming that the Re was above the critical value of 10^5. This had the advantage that a direct comparison of results to those of Eraydin, but had two major disadvantages:

1) **That the observed Re in the flume was not over the critical range, especially if when choosing the higher flow depth of 48cm in the flume.**

2) **The wagon was limited in total length to 1.85m. For the investigation of the effects of multiple bags over such as small distance, the bags themselves should be therefore also small. This will result in drag force readings in which fluctuations due to the ambient flow field might be greater than those observed due to the change in the experimental setup itself.**

For these reasons, it was decided to carry out the multiple bag experiments using an L_r of 10.

Table 4.1: *Flume flow properties for varying depths and flow rates. The Re should be >27,000 for turbulent flow and Re_{crit} should be above 10^5. An Fr < 1 indicates that in all cases the flow was subcritical.*

Flow Rate in Flume [l/s]	Depth (z) [cm]	Re [-]	Fr_{max} [-]
150	48	1.18-1.37 E+5	0,052
150	38	1.22-1.40 E+5	0,076
120	48	0.96-1.06 E+5	0,040
120	38	0.97-1.11 E+5	0,060
90	48	0.09-1.75 E+5	0,032

Flows which are dominated by pressure forces and inertial reactions and which have negligible viscous and gravitational components can be characterized by the Euler number, Eu [7]. The Eu is considered to be solely a function of the shape of the flow boundaries. An additional benefit of using the Eu is that it is independent of values of model size, flow velocity, fluid density and of the reference pressure. An important requirement for drag force models using the Eu is that the Re must be high enough to account for complete boundary flow separation over the submerged body. That is, the Re must be larger than Re_{crit}, which here is taken as $Re>10^5$.

In order to find out if the Euler model law is valid for the experiments carried out in this work, the results of the drag force from using L_r 5 were compared to those of L_r 10. If the flow is independent of the effects of viscous forces, then twice the difference should be observed. Comparison of the two cases however, revealed that since the experiments were carried out within the Re_{crit} range, the forces do not double with the doubling of the geometric properties. Principally, this means that the drag force obtained is both a function of the geometry and the Re [10]. Despite of this fact the higher L_r was chosen in order to increase the allowable bag spacing for multiple bag experiments. However, the effect of geometry cannot be fully established unless C_d versus a wide range of possible Re is further examined. The available range of flow velocities in the flume was simply too small to do so in this case. Additionally, since there is no single specific case for a natural system in which the drag forces are to be compared, it was assumed that in nature the Re will be sufficiently high enough to overcome Re_{crit} in most practical applications.

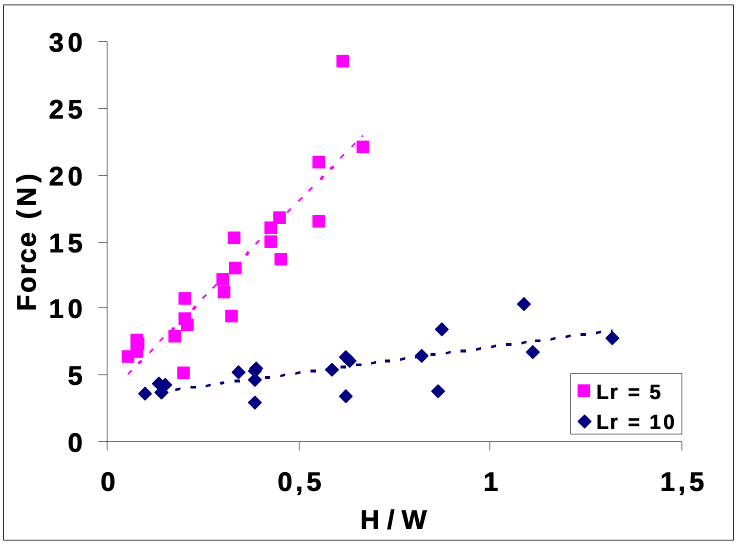

Figure 4.8: *Force versus height to width ratio for two different model lengths. This relationship for application of the Euler model law is not valid in this case.*

4.2.2 Single Bags

A series of tests were run in the flume to find out what geometric configuration generated the best drag force. Both $L_r = 5$ and $L_r = 10$ were used with the flume depth fixed at 48cm. Performance was analyzed by fixing various areas perpendicular to the flow direction and measuring the drag force as the bag was moved in 5cm increments vertically in the flume.

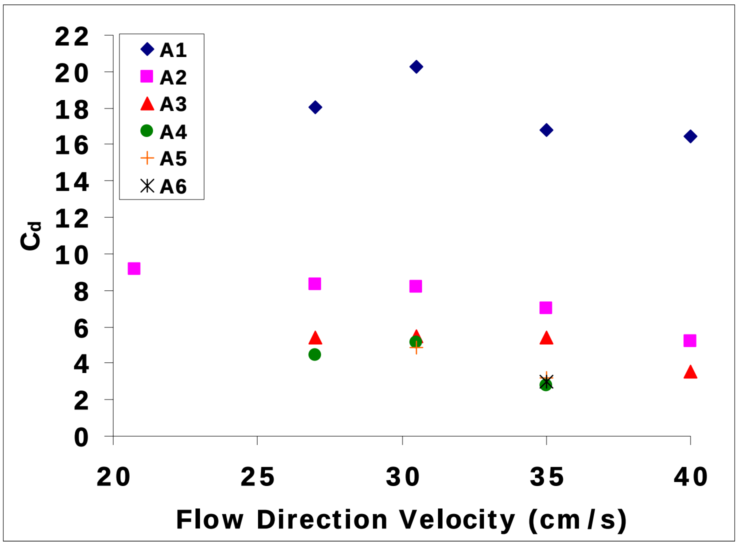

Figure 4.9: *C_d versus Flow Velocity varying Area for a model L_r of 10. Note the "Hummer-like" drag coefficients for the smallest areas.*

Table 4.2: *Results of drag coefficient testing on a single textile bag with an L_r of 10. The maximum drag force does not correspond to the maximum area due to the hydrodynamic properties of the system. Thus, the bag with the largest C_d is not the best choice.*

Area L_r = 10	Total Area [m^2]	C_d Max [-]	$F_{d\ Max}$ [N]
A1	5,9E-03	20,2	6,7
A2	1,5E-02	9,2	7,9
A3	2,5E-02	5,5	8,7
A4	3,5E-02	5,1	10,8
A5	4,5E-02	4,8	12,7
A6	5,4E-02	3,0	10,1

It is most important to look at the results of the findings critically. First the previously described geometric ratios need to be taken into account. It has already been established that for rectangular bodies, the amount of available area per change in perimeter changes rapidly. Additionally, the drag coefficient can be considered essentially as ratio of force generated to its area, for velocities much less than one. This means that for apparently very high C_d values, (especially those over 10) the amount of force per area is simply large not because the force is large, but because the area is very small. Conceptually this may sound strange, but for a unit force with a velocity of 0.1m/s compared to a system which has a similar area and also produces a unit force with 1m/s, the resulting drag coefficient would be different by a factor of 100. An additional consideration is that the textile bags garnering the highest drag coefficients were bags which were long and in most cases unstable.

Looking only at the amount of theoretical force generated per length of the bag in the flow direction, it becomes quickly apparent that a very long turbine would be needed in order to make use of those bags with the highest C_d. Put simply, the drag coefficient can be seen as an indicator of how much force can be generated in terms of both the length of the turbine, and the height of the bag. Therefore the COP approach as used by Eraydin will also be applied here, since it is obvious that otherwise the textile turbine experiences an over-unity energy production! The best performance for a single textile bag was for flat plate rectangular bags with an H/W ratio of 0.67 submerged fully into the vertical portion of the velocity profile.

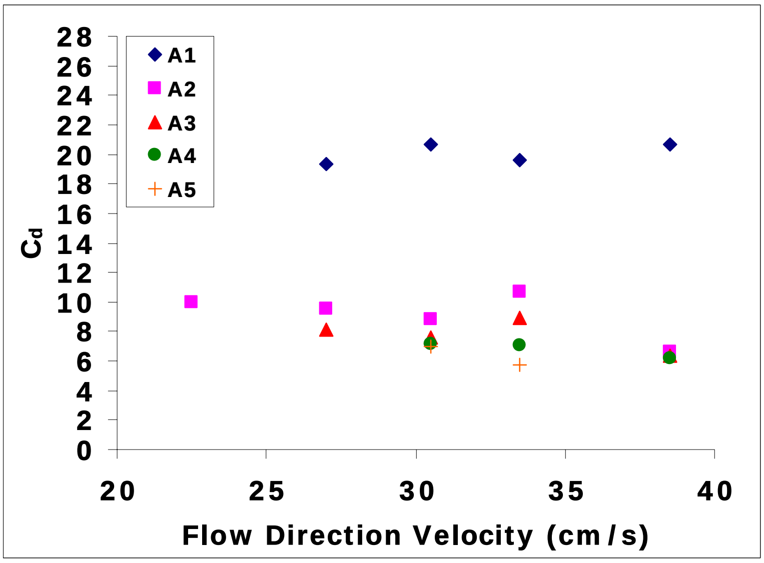

Figure 4.10: *C_d versus Flow Velocity varying Area for a model L_r of 5. The results are in general agreement with those for L_r of 10.*

Table 4.3: *Results of drag coefficient testing on a single textile bag with an L_r of 5. In this case too, the most force was not generated by the configuration which provided the highest C_d.*

Area L_r = 5	Total Area [m^2]	C_d Max [-]	$F_{d\ Max}$ [N]
A1	1,2E-02	27,4	9,9
A2	3,2E-02	10,7	13,1
A3	5,2E-02	8,9	17,6
A4	7,1E-02	7,1	19,1
A5	8,9E-02	7,0	23,3
Max	**8,9E-02**	**27,4**	**23,3**
Min	**1,2E-02**	**7,0**	**9,9**

4.2.3 Multiple Bags

The experiment with multiple bags was by far the most interesting. It was decided in order to keep boundary effects due to the flume as minimal as possible to position the bags along the central axis of the flume, at a distance of 50cm from the wall. The flow depth used was 38cm to achieve the highest Re and corresponding flow velocity. All multiple bag trials were conducted using a flow rate of 150 l/s. Multiple bag trials were run with two and three bags, set up in series. The distance between the bags was fixed to be equidistant in trials 1-4 as shown in Figure 4.11. A fifth trial was also run with the first and third bags remaining at a constant distance from one another at 1.6m, while the second bag was moved closer to the first. This was done to establish if an asymmetric bag configuration along the length of the flume could lead to a flow regime which might provide a better momentum exchange.

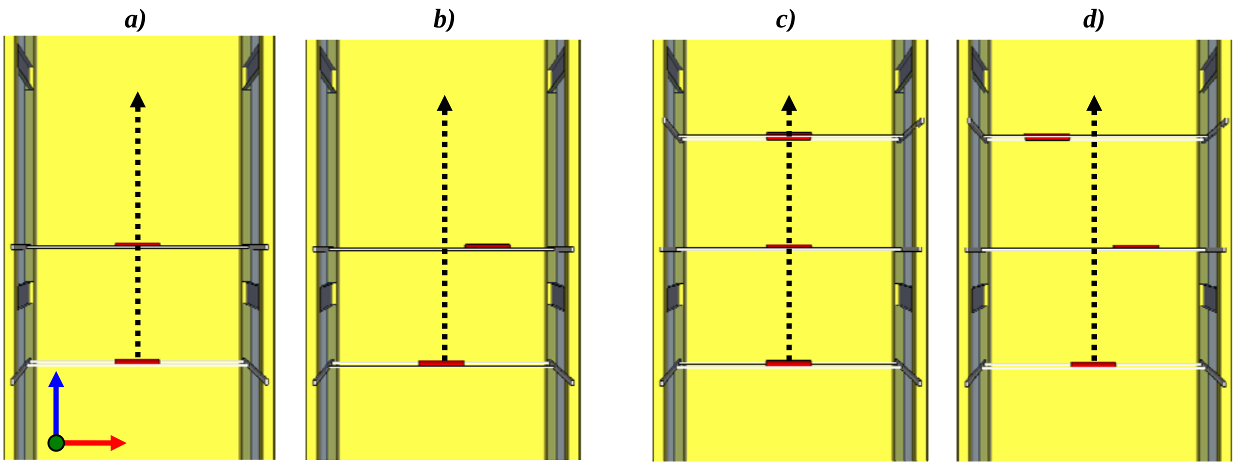

Figure 4.11: Plan view of the experimental setup for multiple bag testing. ***a)*** *2 bags, equidistant spacing,* ***b)*** *2 bags offset from first bag edge,* ***c)*** *3 bags, equidistant spacing,* ***d)*** *3 bags, staggered offset from first bag edge. The black arrow is from the centre of the first bag.*

Trials two and three were also run including an offset, along the horizontal axis as seen in Figure 4.11. This was considered because it was observed that the flow accelerates around the first bag in the system, and it was thought that an enhanced momentum exchange could be obtained if the second and third bags were not placed directly behind first to benefit from the local flow acceleration.

4.3 RESULTS

It was observed that applying a horizontal offset of the bags such as the one used in this experiment resulted in an almost constant value of the total system drag, independent of the distance between bags. The height of the bag used in the experiments was fixed to 15cm, meaning that for every 15cm moved downstream, the x/h ratio increases by a value of one.

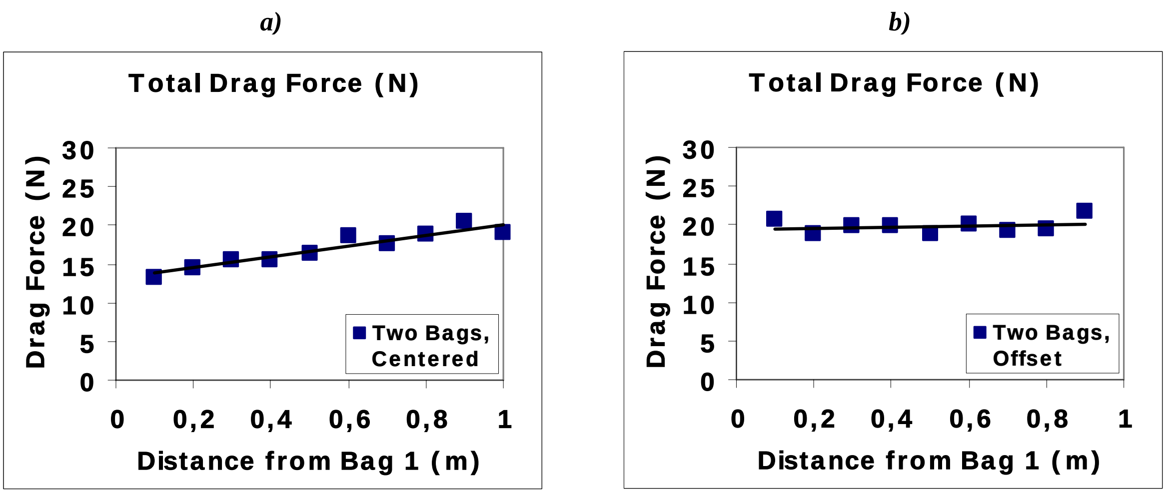

Figure 4.12: *Results of two textile bags with varying distance from each other. Cases* ***a) - d)*** *here also match those of* ***a) - d)*** *shown above in Figure 4.10.*

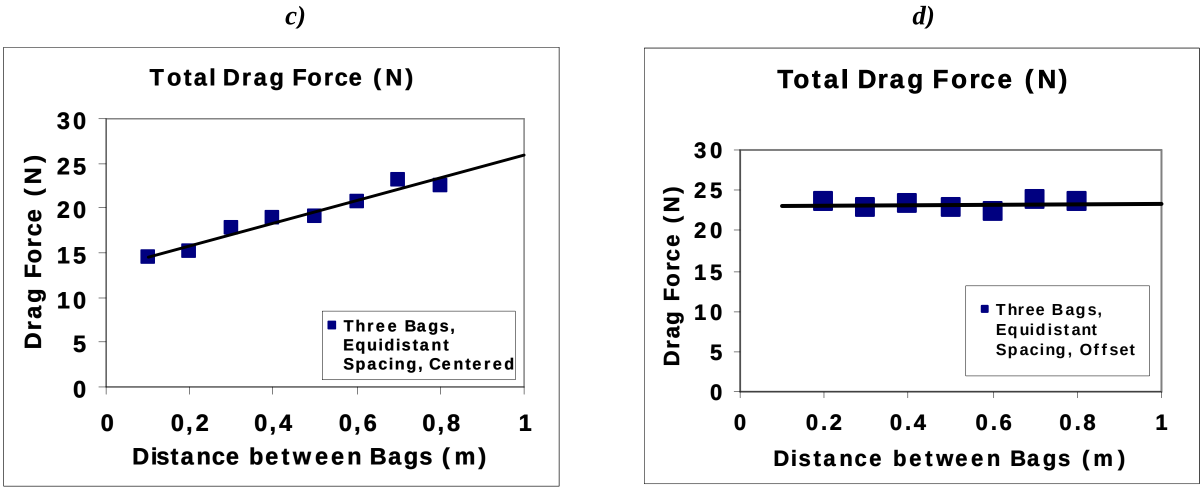

Figure 4.13: *Results of two textile bags with varying distance from each other. Cases **a) - d)** here also match those of **a) - d)** shown above in Figure 4.10.*

Fixing the maximum distance between bags at 1.6m (due to the length of the experimental apparatus) resulted in a maximum testable x/h ratio of greater than 10. This provided the evidence needed to determine that a consistently high value of the drag coefficient using multiple bags with equidistant longitudinal spacing from $0.7<h<10$ can be achieved. The exact location of the maximum depends highly on the flow regime in the system, and the specific configuration of the bags. Most importantly it can be noted that the variation of the maximum as seen in Figure 4.13 (d) varies only slightly. Thus, for the offset case the number of textile bags can be reduced for a given total textile turbine length.

One question remains: Why at a spacing of only 10cm away from the next bag is the same overall system drag found as when we are spaced 100cm away? The conclusion the author came to is that as the bags move closer to the first bag, the momentum transfer from one bag to the other increases linearly, and at approximately the same rate at which for centred bags the transfer decreases. This assumption should be checked using the numerical model, where it is possible to break out the components of the drag force for each individual bag.

4.4 ERROR

Since essentially the same experimental procedure was used in this work as that of Eraydin, the same relative error of 10% can be assumed. It may be possible that a slight reduction of this occurs, because a larger sample of depth-averaged velocities were used in the estimation of C_d. Additionally, the experimental apparatus for this work was more stable, and the force measurement was done in only the x-direction to further reduce error. To be conservative, assuming a 10% relative error is a safe assumption.

CHAPTER 5

CONCLUSIONS

This section of the report contains the conclusions for only the experimental works. Since the Euler Model did not apply, the establishment of a specific C_d – Re relationship for the prototype was not possible. However, ranges of COPs were obtained which can then be used in estimating power generation of a prototype. From this work, the following conclusions can be made:

- Flat, vertical, plate-shaped textile bags which are offset horizontally from one another provide the best total system drag.

- Using a horizontal offset makes the system drag independent of x/h for practical ranges of use (the bags are not expected to be < 10cm apart from one another).

- Placing the textile bag vertically in the region with the highest flow velocity can increase the overall drag force by up to 10% (in the experiment this was the maximum value, in a natural river or stream variation from this can be expected). Previously, in both the prototype experiments in a natural environment and in the laboratory work it was assumed that the bags should be at the surface. It is recommended that for future prototype work, a depth-varied flow velocity profile is first taken to assess the most suitable vertical positioning of the bags.

- The bag shapes providing the highest drag coefficients (C_d>20) were those which were extremely thin and which allowed the bag material to tail. This bag shape is not practical since it can only generate very little force per length of the turbine. It is therefore recommended to use bags with a rectangular-shaped opening having as little trailing material as possible.

- Coefficients of performance for multiple bags ranged from 150 for flat, plate-like geometries with h/w ratios of 0,65 to 300 for h/w ratios of 0.2. This varies from theory, which states that the best drag for a single bag should come from the 0.65 ratio. The author assumes this is due to the effects of the turbulent exchange on the drag coefficient.

- In general, a COP of 150 should be the available minimum for a system with offset flat plate-like construction. This is still much higher than that of any water wheel.

- Work done by Higuchi et al. [6] investigating the drag force during parachute inflation has indicated that during the rapid opening of flexible membranes, the resulting drag force can be 6-8 times that of the steady-state case. This indicates that perhaps a textile turbine which takes advantage of the bag inflation drag force exclusively may yield even better results.

In conclusion, the focus of future work should be performed on assessing the characteristics of the system while under motion. The flow regime around bags in motion, and the stability of a floating device are still key questions which need to be answered.

REFERENCES

[1] AUFLEGER M., NIEDERMAYR A.: *V-Rampen und deren Verwendung in Kombination mit Ufferrückbaumaßnahmen* In: Wasserwirtschaft 11 (2006), pp. 20-21.

[2] BOHL W. 2005. *Technische Strömungslehre.* Vogel.504 pp.

[3] BOYLE G. 1996. *Renewable Energy: Power for a Sustainable Future* Oxford: Oxford University Press. 479 pp.

[4] ERAYDIN H. 2006 Investigation on a new type of turbine. (Master's Thesis) Institute für Wasserbau, Universität Stuttgart, Germany

[5] GERHARDT H. J., GOWDA B. H. L. & KRAMER C. 1985 Pressure field around three-dimensional bluff bodies. *Applied Scientific Research.* **42,** pp. 245-263.

[6] HIGUCHI H., STRICKLAND J. H. & PETERSON C. W. 1996 The fluid dynamics of parachute inflation. *Annu. Rev. Fluid Mech.* **28,** pp. 361-87.

[7] KOBUS, H. 1980. *Hydraulic Modelling.* DVWK Bulletin 7: 172 pp.

[8] MAYS L. W. 2001. *Water Resources Engineering.* New York: John Wiley & Sons. 761 pp.

[9] MÜLLER G.: *Die Staudruckmaschine – tatsächlich die Innovative Neuentwicklung?* In: Wasserwirtschaft 11 (2006), pp. 34-35.

[10] OERTEL H. jr., BÖHLE M., DOHRMANN U. 2003. *Übungsbuch Strömungsmechanik.* Wiesbaden: Vieweg. 333 pp.

[11] OERTEL H. jr. 2001. *Introduction to Fluid Mechanics: Fundamentals and Applications.* Wiesbaden: Vieweg. 167 pp.

[12] PARKINSON G. V. & YEUNG W. W. H. 2000 Base pressure predictions in bluff-body potential-flow models. *J. Fluid Mech.* **423,** pp. 381-394.

[13] THAKE J. 2000. *The Micro-Hydro Pelton Turbine Manual: Design, Manufacture, Installation, for Small-scale Hydropower* Southampton Row, London: ITDG. 180 pp.

[14] University of Southampton, School of Engineering Sciences April 7th, 2007. *Design Tips-boundary layers.*, http://www.soton.ac.uk/ses/outreach/greenpower/boundarylayers.html.

[15] Wikipedia December 7th, 2006. *Drag coefficient.*, http://en.wikipedia.org/wiki/Drag_coefficient.

[16] ZIEREP J. 1993. *Grundzüge der Strömungslehre.* Springer. 171 pp.